

## Structural, optical, and electrical properties of Yb-doped ZnO thin films prepared by spray pyrolysis method

I. Soumahoro, G. Schmerber, A. Douayar, S. Colis, M. Abd-Lefdil, N. Hassanain, A. Berrada, D. Muller, A. Slaoui, H. Rinnert, and A. Dinia

Citation: *Journal of Applied Physics* **109**, 033708 (2011); doi: 10.1063/1.3544307

View online: <https://doi.org/10.1063/1.3544307>

View Table of Contents: <http://aip.scitation.org/toc/jap/109/3>

Published by the [American Institute of Physics](http://www.aip.org)

---

### Articles you may be interested in

[A comprehensive review of ZnO materials and devices](#)

*Journal of Applied Physics* **98**, 041301 (2005); 10.1063/1.1992666

[Green luminescent center in undoped zinc oxide films deposited on silicon substrates](#)

*Applied Physics Letters* **79**, 943 (2001); 10.1063/1.1394173

[On the optical band gap of zinc oxide](#)

*Journal of Applied Physics* **83**, 5447 (1998); 10.1063/1.367375

[Fabrication of green and orange photoluminescent, undoped ZnO films using spray pyrolysis](#)

*Journal of Applied Physics* **84**, 2287 (1998); 10.1063/1.368295

[Optical and electrical properties of ZnO films prepared by spray pyrolysis for solar cell applications](#)

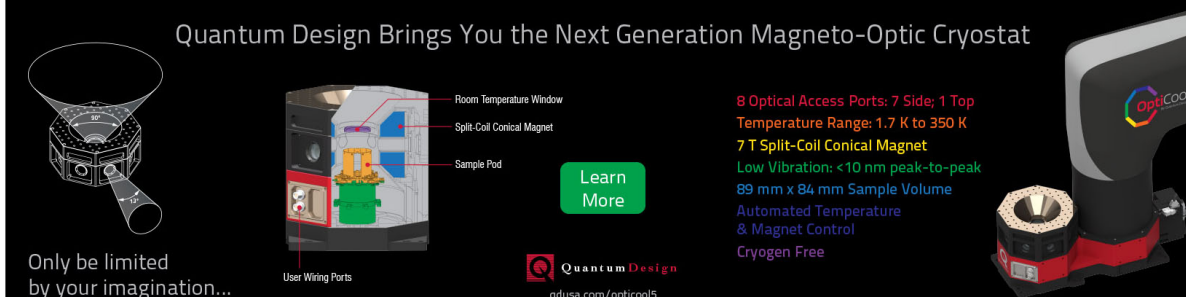
*Journal of Vacuum Science and Technology* **16**, 994 (1979); 10.1116/1.570167

[Antireflective downconversion ZnO:Er<sup>3+</sup>, Yb<sup>3+</sup> thin film for Si solar cell applications](#)

*Journal of Applied Physics* **117**, 055301 (2015); 10.1063/1.4906976

---

Quantum Design Brings You the Next Generation Magneto-Optic Cryostat



The advertisement features a central cutaway diagram of the cryostat with labels: Room Temperature Window, Split-Coil Conical Magnet, Sample Pod, and User Wiring Ports. To the left is a 3D perspective view of the device. To the right is a photograph of the physical cryostat with the 'OptiCool' logo. A 'Learn More' button is positioned below the cutaway diagram.

Only be limited by your imagination...

Learn More

Quantum Design  
qdusa.com/opticool5

8 Optical Access Ports: 7 Side; 1 Top  
Temperature Range: 1.7 K to 350 K  
7 T Split-Coil Conical Magnet  
Low Vibration: <10 nm peak-to-peak  
89 mm x 84 mm Sample Volume  
Automated Temperature & Magnet Control  
Cryogen Free

# Structural, optical, and electrical properties of Yb-doped ZnO thin films prepared by spray pyrolysis method

I. Soumahoro,<sup>1,2,3</sup> G. Schmerber,<sup>2</sup> A. Douayar,<sup>1</sup> S. Colis,<sup>2</sup> M. Abd-Lefdil,<sup>1</sup> N. Hassanain,<sup>1</sup> A. Berrada,<sup>1</sup> D. Muller,<sup>3</sup> A. Slaoui,<sup>3</sup> H. Rinnert,<sup>4</sup> and A. Dinia<sup>2,a)</sup>

<sup>1</sup>Laboratoire de Physique des Matériaux, Faculté des Sciences, B.P. 1014, Rabat, Morocco

<sup>2</sup>IPCMS, UMR CNRS 7504, UDS-ECPM, 23 rue du Loess, B.P. 43, F-67034 Strasbourg, France

<sup>3</sup>InESS, UMR CNRS 7163, UDS, 23 rue du Loess, B.P. 43, F-67037 Strasbourg, France

<sup>4</sup>Institut Jean Lamour, Nancy-University-UPVM-CNRS, Boulevard des Aiguillettes B.P. 239, 54506 Vandœuvre-lès-Nancy Cedex, France

(Received 19 September 2010; accepted 6 December 2010; published online 3 February 2011)

Yb-doped ZnO thin films were prepared on glass substrates by spray pyrolysis technique in order to investigate the insertion of Yb ions in the ZnO matrix and the related optical properties of the films. The molar ratio of Yb in the spray solution was varied in the range of 0–5 at. %. X-ray diffraction patterns showed that the undoped and Yb-doped ZnO films exhibit the hexagonal wurtzite crystal structure with a preferential orientation along [002] direction. No secondary phase is observed in Yb-doped ZnO films. All films exhibit a transmittance between 75 and 90% in the visible range with a sharp absorption onset about 375 nm corresponding to the fundamental absorption edge at 3.3 eV. The photoluminescence measurements show a clear luminescence band at 980 nm that is characteristic of Yb<sup>3+</sup> transition between the electronic levels <sup>2</sup>F<sub>5/2</sub> and <sup>2</sup>F<sub>7/2</sub>. This is an experimental evidence for an efficient energy transfer from ZnO matrix to Yb<sup>3+</sup>. Hall effect measurements showed low resistivities and high carrier mobilities which makes these films of interest to photovoltaic devices. © 2011 American Institute of Physics. [doi:10.1063/1.3544307]

## I. INTRODUCTION

Large band gap semiconductors based on metallic oxides show an increasing interest due to their wide range of applications in the field of spintronics, information storage, optoelectronics, and photovoltaic devices.<sup>1–5</sup> Rare-earth (RE)-doped wide band gap materials are particularly of potential interest to reach the down conversion function. The idea is to reduce the thermalization losses occurring in solar cells by transforming a high energy photon into two photons of lower energy. In such materials absorption of photons takes place via excitation of the host material. Auger processes and energy transfer processes between the host matrix and the doping ions are able to involve in the excitation of two RE ions after only one incoming photon. On the other hand, a theoretical study has shown that it is possible to increase the conversion efficiency of solar cells up to 35–40% by adding a down conversion wide band gap semiconducting oxide doped with RE ions at the top of a silicon-based conventional solar cell.<sup>6</sup> This perspective has led to (i) an intense research activity on these types of materials and to (ii) a renew of the interest for the deposition techniques such as sol-gel,<sup>7</sup> sputtering,<sup>8</sup> and electroplating<sup>9</sup> which are commonly used at industrial scale. The nature of the host matrix is chosen to correspond to the required transparency to visible and near infrared (IR) light, to be compatible with silicon (i.e., to allow the absorption of photons with the energy higher than the band-gap of silicon) and RE (i.e., to show an efficient energy transfer to the RE ions).<sup>10,11</sup>

Among the promising materials, ZnO holds a particular

position since it combines both semiconducting and optical properties, with potential impact in the light conversion into electric power. Moreover ZnO is non-toxic, abundant and has a wide band-gap (3.3 eV), a high transparency for visible light, and a large energy of the exciton binding energy at room temperature (~60 meV).<sup>12</sup> It is also well known that the doping of ZnO with trivalent RE ions enhances the optical activity and that the low phonon energy (~436 cm<sup>-1</sup>) renders this matrix favorable for the RE luminescence.

In this study we have focused our interest on Yb doped zinc oxide (ZnO:Yb). Doping by Yb is motivated by the characteristic optical transition around 980 nm of Yb<sup>3+</sup> ions<sup>13</sup> which is compatible with Si-based solar cells. Samples have been prepared by spray pyrolysis and studied by x-ray diffraction (XRD) experiments, absorption and photoluminescence (PL) spectroscopies. It is shown that an efficient energy transfer between Yb ions and the ZnO matrix allows us to obtain the near IR PL of Yb ions.

## II. EXPERIMENTAL

Zn<sub>1-x</sub>Yb<sub>x</sub>O (0 ≤ x ≤ 0.05) thin films were deposited on glass substrates by spray pyrolysis technique. An homogeneous solution was prepared by dissolving zinc chloride (ZnCl<sub>2</sub>) (0.05 M) and hexahydrated ytterbium chloride (YbCl<sub>3</sub>·6H<sub>2</sub>O) in distilled water at room temperature. The solutions have 0, 1, 3, and 5 at. % Yb molar ratio. Some drops of acetic acid (CH<sub>3</sub>COOH) have been added while stirring at room temperature for 30 min to obtain a clear solution. The glass substrate was cleaned in ethanol, rinsed in distilled water, and subsequently dried under nitrogen gas flow before deposition. The substrate was then placed on a

<sup>a)</sup>Electronic mail: aziz.dinia@ipcms.u-strasbg.fr.

plate and heated progressively until the deposited temperature is reached. All films were deposited at 350 °C during 77 min with a flow rate of the solution fixed at 2.6 ml/min.

The structural properties of the films were analyzed using a Bruker D8 Advance x-ray diffractometer equipped with a Cu  $K\alpha_1$  monochromatic source ( $\lambda=1.54056$  Å). The surface morphology has been observed using a JEOL JSM-6700F scanning electron microscope (SEM) coupled with an energy dispersive x-ray spectroscopy (EDX) analyzer used to determine the chemical composition of the films. The distribution of the chemical elements (Zn, Yb, O) along the growth direction as well as the thickness of the films were investigated by Rutherford backscattering spectroscopy (RBS). The RBS technique is based on elastic scattering collision between high energy (2.9 MeV) incidents He ions and the stationary atoms located in the sample. This technique allows investigating the atomic distribution (i.e., the stoichiometry) as a function of depth in the film.

The optical properties of the films were checked by using a U-Perkin-Elmer Lambda 950 spectrophotometer for the absorption (in transmission and reflectance modes) measurements. PL measurements were also performed in order to have insight on the film defects and on the spectral transitions of  $\text{Yb}^{3+}$ . For PL experiment in the visible range, the 355 nm excitation line is delivered by a frequency-tripled neodymium-doped yttrium aluminium garnet (Nd-YAG) laser. For the steady state PL experiments in the near IR range, the samples were excited by a 30 mW He–Cd laser using the 325 nm line. For the time-resolved PL experiments, the samples were pumped by the 355 nm line of a frequency-tripled Nd-YAG laser. The laser pulse frequency, energy and duration were typically equal to 10 Hz, 50  $\mu\text{J}$ , and 20 ns, respectively. The PL signal was analyzed by a monochromator equipped with a 600 grooves/mm grating and by a photomultiplier tube cooled at 190 K. The spectral response of the detection system was precisely calibrated with a tungsten wire calibration source. PL experiments were performed at room temperature and at 77 K for the near IR spectral range. The electrical properties of films were studied at room temperature using an ECOPIA Hall effect measurement system.

### III. RESULTS AND DISCUSSIONS

Figure 1 shows the XRD patterns of the  $\text{Zn}_{1-x}\text{Yb}_x\text{O}$  ( $0 \leq x \leq 0.05$ ) thin films. It is clearly seen that only the peaks corresponding to the ZnO wurtzite structure are observed. The samples are polycrystalline, with no sign of spurious

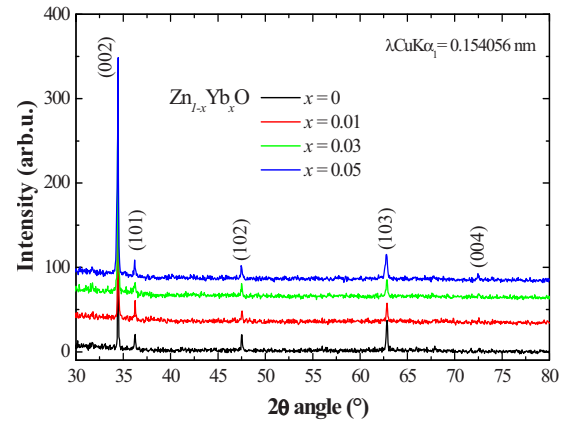


FIG. 1. (Color online) XRD patterns of  $\text{Zn}_{1-x}\text{Yb}_x\text{O}$  ( $0 \leq x \leq 0.05$ ) thin films deposited by spray pyrolysis on glass substrates recorded using a monochromatic Cu  $K\alpha_1$  ( $\lambda=1.54056$  Å) radiation.

phases. The analysis of the peaks intensity shows that all films have a preferential orientation along the [002] direction. The slight decrease in the  $2\theta$  value of the (002) peak for the  $\text{Zn}_{1-x}\text{Yb}_x\text{O}$  films compared to that of the pure ZnO indicates that the c-axis lattice parameter increases with Yb doping which is consistent with other works dealing with the effect of doping in ZnO.<sup>14–16</sup>

Quantitative information concerning the preferential crystallite orientation along the [002] direction is obtained from the analysis of the different texture coefficient (TC) (hkl) associated to the texture of a particular plane. Its deviation from unity indicates a stronger preferred growth along the [hkl] direction. TC is defined as:<sup>17</sup>

$$\text{TC}(hkl) = \frac{I(hkl)/I_0(hkl)}{(1/n)\sum_n I(hkl)/I_0(hkl)},$$

where  $I(hkl)$  is the measured relative intensity of a plane (hkl),  $I_0(hkl)$  is the standard intensity of the plane (hkl) taken from Joint Committee for Powder Diffraction Standard data (Card No. 80-0075), and  $n$  is the number of diffraction peaks. The values of  $\text{TC}(002)$  are reported in Table I. As can be observed, the “textured” character of the samples increases upon Yb doping and remains constant for Yb concentrations larger than 3%. The fact that above 3% the value of  $\text{TC}(002)$  remains rather constant is probably due to the insertion of Yb in interstitial positions related to the low solubility limit of Yb in ZnO. A similar behavior can be also evidenced when considering the crystallite size as a function of the Yb concentration. This size calculated from the (002) diffraction line [ $D_{(002)}$ ] using the Scherrer’s formula<sup>18</sup> is

TABLE I. Various parameters of  $\text{Zn}_{1-x}\text{Yb}_x\text{O}$  ( $x=0, 0.01, 0.03, 0.05$ ) thin films.

x nominal	RBS		XRD		Optical measurements	
	Thickness (nm)	Effective $x \pm 0.005$	TC(002)	$D_{(002)}$ (nm)	$H_R$	Gap energy (eV)
0.00	410 ± 40	0	2.71	92(5)	0.41	3.27(2)
0.01	250 ± 25	0.009(1)	3.05	83(5)	0.42	3.27(2)
0.03	455 ± 45	0.023(2)	3.28	69(4)	0.56	3.23(2)
0.05	455 ± 45	0.039(3)	3.15	83(5)	0.84	3.22(2)

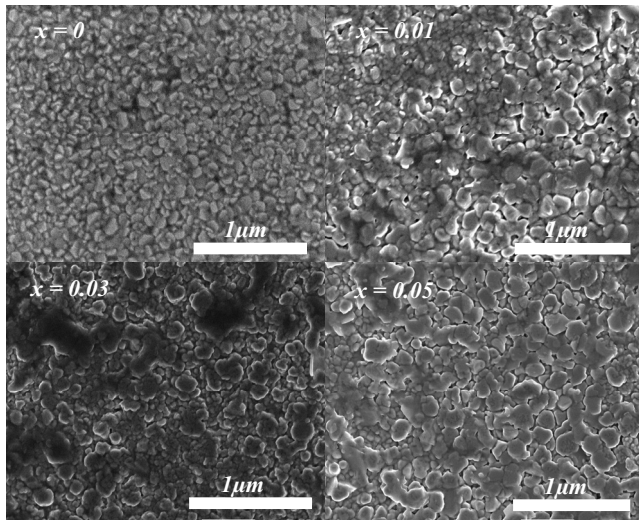


FIG. 2. SEM images of  $Zn_{1-x}Yb_xO$  ( $0 \leq x \leq 0.05$ ) thin films deposited by spray pyrolysis on glass substrates.

shown in Table I. The size decreases rapidly from 92 to 69 nm when the Yb concentration increases to 3%. Besides the solubility limit of Yb in ZnO, this also suggests that Yb acts as nucleation centers as long as Yb substitutes Zn ions in the ZnO matrix. Due to this low solubility limit, the lattice parameters  $a$  and  $c$  of about 0.3279 nm and 0.5248 nm, respectively, did not show any variation for Yb concentration larger than 3%.

Figure 2 shows SEM images obtained for different  $Zn_{1-x}Yb_xO$  ( $x=0, 0.01, 0.03, 0.05$ ) thin films. We can note that all the films are fairly uniform and homogeneous. The chemical composition of the films has been determined using EDX in different regions of the films surface. The results show systematically larger Yb concentration with respect to the nominal concentration.

The RBS spectra recorded for the  $Zn_{1-x}Yb_xO$  ( $x=0, 0.01, 0.03, 0.05$ ) are shown in Fig. 3. The spectra show as expected the contributions of oxygen, silicon (from the substrate), zinc, and ytterbium. The Yb RBS line (at about 2.65 MeV) recorded for  $Zn_{1-x}Yb_xO$  increases as expected with the Yb concentration. However, this line as well as the

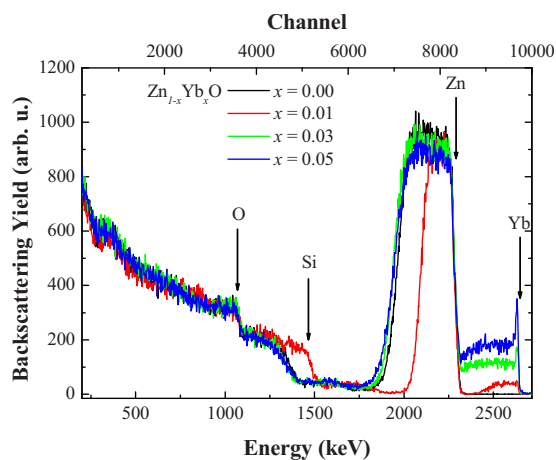


FIG. 3. (Color online) RBS spectra of the  $Zn_{1-x}Yb_xO$  ( $0 \leq x \leq 0.05$ ) thin films deposited by spray pyrolysis on glass substrates.

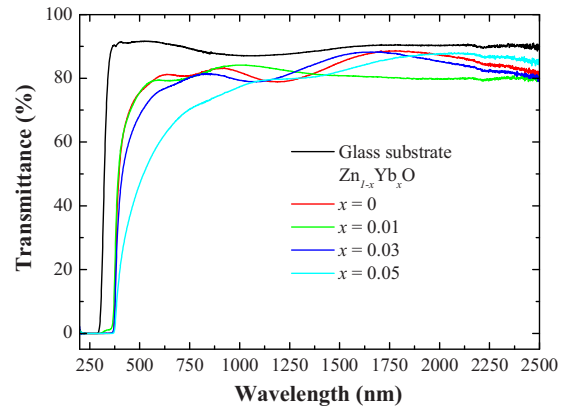


FIG. 4. (Color online) Transmittance spectra of  $Zn_{1-x}Yb_xO$  ( $0 \leq x \leq 0.05$ ) thin films deposited by spray pyrolysis on glass substrates.

Zn one, presents a rather smooth variation in the low energy part. This suggests a significant interface (substrate/film) roughness of the deposited films, in contrast to the surface roughness characterized by an abrupt variation in the RBS signal. It is also important to point out the existence in the high energy side of the Yb line, of a sharp peak in a region representing about 10 nm from the surface. This peak, which starts to be visible in the 3% Yb doped sample, is more pronounced for higher Yb concentration, and can be related to the low solubility limit of Yb in ZnO. Although most Yb ions remain distributed in the film, more and more ions migrate toward the film surface. In contrast to EDX analyses, the Yb concentrations estimated by RBS are smaller than the nominal ones. These values, together with the film thicknesses estimated by RBS are given in Table I.

The transmittance (Fig. 4) and total reflectance (diffusion, and specular contributions) (not shown here) of  $Zn_{1-x}Yb_xO$  ( $0 \leq x \leq 0.05$ ) thin films was measured in the 200–2500 nm wavelength range. All the films exhibit a high transmittance between 75 and 90% in the visible range except for high doping content where the transmittance decreases drastically. The specular transmittance was also measured and its contribution was very small (around 5%). The absence of contrasted fringes is related to the diffusion phenomenon in agreement with the small grain size. The haze ratio  $H_R$  is evaluated by the ratio of the diffused reflectance to the total reflectance of  $Zn_{1-x}Yb_xO$  films at the wavelength of 550 nm.  $H_R$  increases from 0.41 to 0.84 when Yb content increases from 0 to 0.05 (Table I) which indicates a non negligible roughness at the surface of the films in agreement with RBS and SEM analyses.

The plots of  $(ah\nu)^2$  versus  $(h\nu)$  for the various Yb doped ZnO samples, and the extrapolation of the linear portion of the plots onto the energy axis gave the band gap value. We observed a slight decrease from 3.27 to 3.22 eV with increasing Yb doping from 0 to 5 at. %. This result is in agreement with what was observed in Fe, Mn, or Co doped ZnO films grown by ultrasonic spray pyrolysis and other techniques.<sup>19–25</sup>

PL measurements are very useful because they allow showing the energy levels due to defects in the ZnO matrix, as already reported by Behera *et al.*<sup>26</sup> Figure 5(a) shows the PL spectra at room temperature of undoped and Yb doped



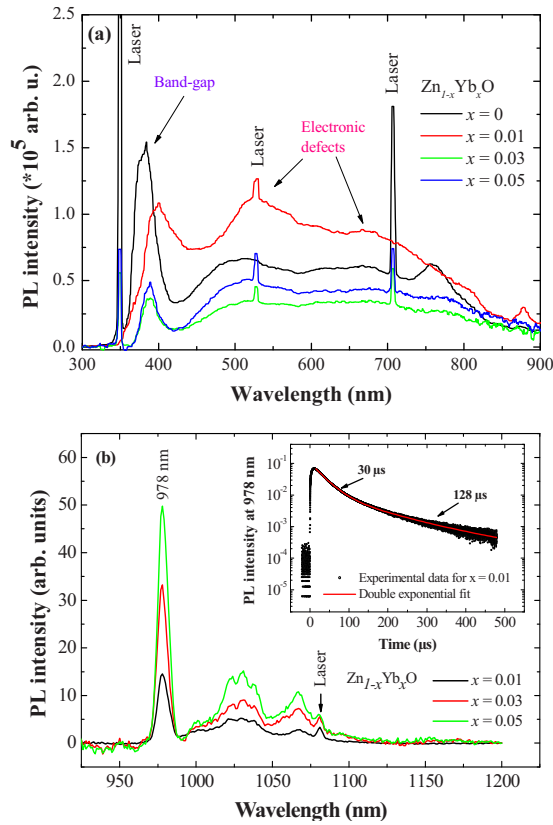


FIG. 5. (Color online) (a) PL at room temperature in the visible region of  $\text{Zn}_{1-x}\text{Yb}_x\text{O}$  ( $0 \leq x \leq 0.05$ ) thin films. (b) PL at 77 K of  $\text{Zn}_{1-x}\text{Yb}_x\text{O}$  ( $0 \leq x \leq 0.05$ ) thin films measurements in the IR region showing the transition lines of  $\text{Yb}^{3+}$  between the levels  ${}^2\text{F}_{5/2}$  and  ${}^2\text{F}_{7/2}$ . The inset shows the time-dependent PL emission at 978 nm, measured at 77 K.

$\text{ZnO}$  films. Thus, although PL is excited by the frequency-tripled YAG: $\text{Nd}^{3+}$  laser at 1064 nm, a weak contribution of the doubled frequency line is responsible for the peak at 532 nm of the PL spectrum. The peak at 710 nm corresponds to the second order diffraction peak of the 355 nm laser line. The strong luminescence band at 379 nm corresponds to the excitonic emission. The electrons from the valence band (VB) are excited to the conduction band and upon emitting the same amount of energy; they come back to the VB and associate with a hole to form an exciton. The second order of this PL band is visible at 760 nm. The wide PL bands centered at 510 and 680 nm are characteristic of deep levels of oxygen vacancies in the  $\text{ZnO}$  matrix, and zinc interstitial position, as this was previously observed for  $\text{ZnO}$  thin films prepared by sol-gel method.<sup>27</sup> In addition the PL band of the sample with 1% of Yb is redshifted with respect to the PL of the other samples. This could be related to a higher interstitial Zn amount in the thin sample ( $\text{Zn}_{0.99}\text{Yb}_{0.01}\text{O}$ ) with respect to the other samples.

Figure 5(b) shows the PL in the 900–1200 nm range, measured at 77 K. A baseline was subtracted to take into account the broad response of the glass substrate. A contribution around 980 nm is clearly observed in this wavelength range for the different values  $x=0.01, 0.03, 0.05$ . This emission is characteristic of the  ${}^2\text{F}_{5/2} \rightarrow {}^2\text{F}_{7/2}$  transition of  $\text{Yb}^{3+}$  ions. The PL intensity is an increasing function of the Yb concentration. This result suggests that no concentration

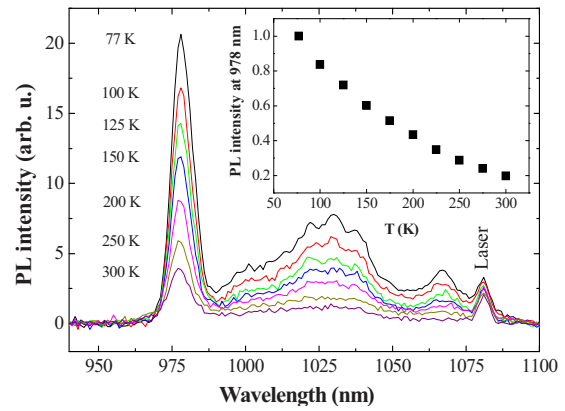


FIG. 6. (Color online) Influence of the temperature on the  $\text{Yb}^{3+}$ -related PL for the  $\text{Zn}_{0.99}\text{Yb}_{0.01}\text{O}$  sample.

quenching effect occurs in this range of doping content. Decay time measurements were performed at 978 nm to confirm that result. The time-dependent PL intensity is shown in the inset of Fig. 5(b) for the sample prepared with  $x=0.01$ . The experimental data are not satisfactorily simulated by a single exponential curve but a good agreement is obtained using a double exponential curve. The existence of the fast contribution is still not clear but could be due the response of the glass substrate. Indeed, only this fast decay component is obtained for a measurement at 950 nm (not shown here) where no  $\text{Yb}^{3+}$ -related PL occurs. Moreover, the decay time is very similar for all the doping content studied here. The decay time is equal to 128, 129, and 150  $\mu\text{s}$  for the Yb content equal to 1, 2, and 5 at. %. This result also suggests that no PL quenching due to non radiative interaction between  $\text{Yb}^{3+}$  ions occurs. As the excitation is not-resonant with  $\text{Yb}^{3+}$  ions levels, the results suggest that the  $\text{Yb}^{3+}$  ions are indirectly excited by the host matrix. This is a strong experimental evidence of an efficient energy transfer from the  $\text{ZnO}$  matrix into the  $\text{Yb}^{3+}$  ion. Further experiments will be performed to further investigate the energy transfer process. Figure 6 shows the  $\text{Yb}^{3+}$ -related PL emission of the sample  $\text{Zn}_{0.99}\text{Yb}_{0.01}\text{O}$  for different temperatures. These results show that Yb related signal is rather complex. Presently  $\text{Yb}^{3+}$  ions have only two spin orbit manifolds levels,  ${}^2\text{F}_{5/2}$ , and  ${}^2\text{F}_{7/2}$ . Due to its  $4f^{13}$  electronic configuration, the screening effect of the  $4f$  electrons for Yb is weaker than that occurring for other RE ions, which induces a more important interaction with the host matrix. The host matrix is responsible of the energy splitting of the fundamental and excited states of  $\text{Yb}^{3+}$  ions. Our results show three different bands centered at 978, 1029 and 1067 nm. These bands probably contain several narrow contributions which are not well resolved here. The different contributions could be due to the existence of several sites for the  $\text{Yb}^{3+}$  ions, to the different crystal field effects and to the contribution of phonons. The PL shape obtained here is very similar to the one obtained in Yb doped GaN layers where PL bands are localized at 989, 1012, and 1042 nm.<sup>28</sup> Moreover, a temperature quenching effect is obtained and is characterized by a decrease in the PL intensity with a factor 5 from 77 K to room temperature, as shown on the inset of Fig. 6.

The carrier concentration  $n$ , the Hall mobility  $\mu$ , and the

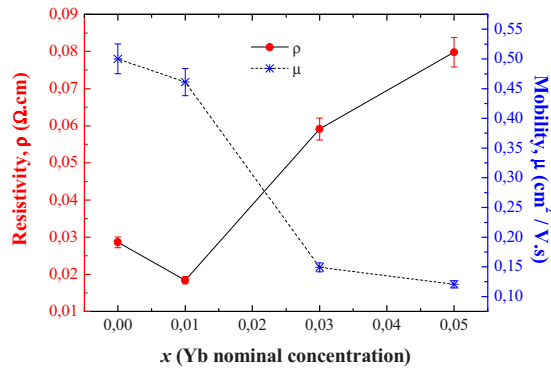


FIG. 7. (Color online) Variation in resistivity and Hall mobility as a function of Yb/Zn ratio ( $x$ ).

electrical resistivity  $\rho$ , were measured at room temperature using the Van der Pauw method.<sup>29</sup> For doped transparent conducting oxides films, carriers originate from intrinsic donors such as lattice defects, from extrinsic doping or from both.<sup>30</sup> In our case, the intrinsic donors are oxygen vacancies and metal atoms in interstitial positions, while the extrinsic doping is due the substitution of Yb for Zn in ZnO structure. One free hole will be produced for every Zn substitution by Yb, which will contribute to the electric conduction of the films as free carriers.

Figure 7 shows the variation in resistivity and Hall mobility as a function of Yb concentration ( $x$ ). All  $\text{Zn}_{1-x}\text{Yb}_x\text{O}$  ( $0 \leq x \leq 0.05$ ) thin films are n-type conducting, indicating that the presence of  $\text{Yb}^{3+}$  in the ZnO matrix is not sufficient to induce a “p” type conduction. The conduction characteristics of ZnYbO thin films are, therefore, primarily dominated by defects in ZnO matrix and that most of Yb atoms are in interstitial positions. This is well supported by RBS results and is in agreement with what was reported by Ungureanu *et al.*<sup>31</sup> and Kaur *et al.*<sup>32</sup> on RE doped ZnO films, Al-doped ZnO films<sup>33</sup> and As-doped ZnCoO films.<sup>16</sup> The carrier density values range between  $6.5 \times 10^{22}$  and  $1.4 \times 10^{21} \text{ cm}^{-3}$ . In addition, both the resistivity and carrier mobility show a small variation with Yb concentration, making these films potentially interesting for their use as photons down conversion layers in photovoltaic cell.

#### IV. CONCLUSION

Polycrystalline  $\text{Zn}_{1-x}\text{Yb}_x\text{O}$  thin films were prepared by spray pyrolysis technique. The structure of the films was not sensitively modified by Yb incorporation. The optical properties were studied by transmittance and reflectance measurements where the transmittance in the visible range was in 75–90% range. A clear Yb related PL peak was observed in the IR region at 980 nm corresponding to  ${}^2\text{F}_{5/2} \rightarrow {}^2\text{F}_{7/2}$  transition indicating an efficient energy transfer from ZnO matrix to the  $\text{Yb}^{3+}$  ions. All  $\text{Zn}_{1-x}\text{Yb}_x\text{O}$  thin films were n-type, and the lowest electrical resistivity was around  $1.8 \times 10^{-2} \Omega \text{ cm}$  for 1% of Yb making these films as potential candidates for photons down conversion process.

#### ACKNOWLEDGMENTS

This work is supported by the program interdisciplinaire énergie du CNRS Grant No. PE10-2.1.2-2.

- <sup>1</sup>S. A. Wolf, D. D. Awschalom, R. A. Buhrman, J. M. Daughton, S. von Molnár, M. L. Roukes, A. Y. Chtchelkanova, and D. M. Treger, *Science* **294**, 1488 (2001).
- <sup>2</sup>E. Fortunato, P. Nunes, A. Marques, D. Costa, H. Águas, I. Ferreira, M. E. V. Costa, M. H. Godinho, P. L. Almeida, J. P. Borges, and R. Martins, *Adv. Eng. Mater.* **4**, 610 (2002).
- <sup>3</sup>T. Moe Borseth, B. G. Svensson, and A. Y. Kuznetsov, *Appl. Phys. Lett.* **89**, 262112 (2006).
- <sup>4</sup>S. Al-Hilli and M. Willander, *Sensors* **9**, 7445 (2009).
- <sup>5</sup>A. Dinia, G. Schmerber, V. Pierron-Bohnes, C. Mény, P. Panissod, and E. Beaurepaire, *J. Magn. Magn. Mater.* **286**, 37 (2005).
- <sup>6</sup>T. Trupke, M. A. Green, and P. Würfel, *J. Appl. Phys.* **92**, 1668 (2002).
- <sup>7</sup>L. Armelao, G. Bottaro, M. Pascolini, M. Sessolo, E. Tondello, M. Bettinelli, and A. Speghini, *J. Phys. Chem. C* **112**, 4049 (2008).
- <sup>8</sup>J. Petersen, C. Brimont, M. Gallart, Guy Schmerber P. Gilliot, C. Ulhaq-Bouillet, J.L. Rehspringer, S. Colis, C. Becker, A. Slaoui, and A. Dinia, *J. Appl. Phys.* **107**, 123522 (2010).
- <sup>9</sup>T. Pauporté, F. Pellé, B. Viana, and P. Aschehoug, *J. Phys. Chem. C* **111**, 15427 (2007).
- <sup>10</sup>E. Alves, L. Kutaras, E. Rita, U. Wahl, and T. Monteiro, *Nucl. Instrum. Methods Phys. Res. B* **206**, 1047 (2003).
- <sup>11</sup>Z. Lin-Li, G. Chang-Xi, and H. Jun-Tao, *Chin. Phys. Lett.* **22**, 1225 (2005).
- <sup>12</sup>S. J. Pearton, D. P. Norton, K. Ip, Y. W. Heo, and T. Steiner, *Prog. Mater. Sci.* **50**, 293 (2005).
- <sup>13</sup>J. L. Yuan, X. Y. Zeng, J. T. Zhao, Z. J. Zhang, H. H. Chen, and X. X. Yang, *J. Phys. D: Appl. Phys.* **41**, 105406 (2008).
- <sup>14</sup>I. Soumahoro, R. Moubah, G. Schmerber, S. Colis, M. Ait Aouaj, M. Abd-lefdil, N. Hassanain, A. Berrada, and A. Dinia, *Thin Solid Films* **518**, 4593 (2010).
- <sup>15</sup>J. Alaria, H. Bieber, S. Colis, G. Schmerber, and A. Dinia, *Appl. Phys. Lett.* **88**, 112503 (2006).
- <sup>16</sup>H. Ndilimabaka, S. Colis, G. Schmerber, D. Muller, J. J. Grob, L. Gravier, C. Jan, E. Beaurepaire, and A. Dinia, *Chem. Phys. Lett.* **421**, 184 (2006).
- <sup>17</sup>S. S. Shinde, P. S. Shinde, S. M. Pawar, A. V. Moholkar, C. H. Bhosale, and K. Y. Rajpure, *Solid State Sci.* **10**, 1209 (2008).
- <sup>18</sup>P. Scherrer, *Göttinger Nachrichten* **2**, 98 (1918).
- <sup>19</sup>U. Alver, T. Kiliç, E. Bacaksiz, and S. Nezir, *Mater. Sci. Eng., B* **138**, 74 (2007).
- <sup>20</sup>Z. C. Chen, L. J. Zhuge, X. M. Wu, and Y. D. Meng, *Thin Solid Films* **515**, 5462 (2007).
- <sup>21</sup>K. J. Kim and Y. R. Park, *Appl. Phys. Lett.* **81**, 1420 (2002).
- <sup>22</sup>S. Colis, H. Bieber, S. Bégin-Colin, G. Schmerber, C. Leuvrey, and A. Dinia, *Chem. Phys. Lett.* **422**, 529 (2006).
- <sup>23</sup>Y. Belghazi, M. Ait Aouaj, M. El Yadari, G. Schmerber, C. Ulhaq-Bouillet, C. Leuvrey, S. Colis, M. Abd-lefdil, A. Berrada, and A. Dinia, *Microelectron. J.* **40**, 265 (2009).
- <sup>24</sup>V. R. Shinde, T. P. Gujar, C. D. Lokhande, R. S. Mane, and S. H. Han, *Mater. Chem. Phys.* **96**, 326 (2006).
- <sup>25</sup>M. Bouloudene, N. Viart, S. Colis, and A. Dinia, *Catal. Today* **113**, 240 (2006).
- <sup>26</sup>D. Behera and B. S. Acharya, *J. Lumin.* **128**, 1577 (2008).
- <sup>27</sup>J. Petersen, C. Brimont, M. Gallart, O. Crégut, G. Schmerber, P. Gilliot, B. Hönerlage, C. Ulhaq-Bouillet, J. L. Rehspringer, C. Leuvrey, S. Colis, A. Slaoui, and A. Dinia, *Microelectron. J.* **40**, 239 (2009).
- <sup>28</sup>W. M. Jadwisieniczak and H. J. Lozykowski, *Opt. Mater.* **23**, 175 (2003).
- <sup>29</sup>D. K. Schroder, *Semiconductor Material and Device Characterization* (Wiley, New York, 1990).
- <sup>30</sup>K. Ellmer, *J. Phys. D: Appl. Phys.* **34**, 3097 (2001).
- <sup>31</sup>M. Ungureanu, H. Schmidt, Q. Xu, H. von Wenckstern, D. Spemann, H. Hochmuth, M. Lorenz, and M. Grundmann, *Superlattices Microstruct.* **42**, 231 (2007).
- <sup>32</sup>R. Kaur, A. V. Singh, and R. M. Mehra, *J. Non-Cryst. Solids* **352**, 2335 (2006).
- <sup>33</sup>L. Li, L. Fang, X. M. Chen, J. Liu, F. F. Yang, Q. J. Li, G. B. Liu, and S. J. Feng, *Physica E* **41**, 169 (2008).